







Facile integration of giant exchange bias in Fe_5GeTe_2 /oxide heterostructures by atomic layer deposition

Jierui Liang ¹, Shanchuan Liang ¹, Ti Xie ¹, Andrew F. May,² Thomas Ersevım,³ Qinqin Wang ¹, Hyobin Ahn,⁴ Changgu Lee ^{4,5}, Xixiang Zhang,⁶ Jian-Ping Wang,⁷ Michael A. McGuire,² Min Ouyang,³ and Cheng Gong ^{1,*}

¹Department of Electrical and Computer Engineering and Quantum Technology Center, University of Maryland, College Park, Maryland 20742, USA

²Materials Science and Technology Division, Oak Ridge National Laboratory, Oak Ridge, Tennessee 37831, USA

³Department of Physics, University of Maryland, College Park, Maryland 20742, USA

⁴SKKU Advanced Institute of Nanotechnology, Sungkyunkwan University, Suwon Gyeonggido 16419, Republic of Korea

⁵Department of Mechanical Engineering, Sungkyunkwan University, Suwon Gyeonggido 16419, Republic of Korea

⁶King Abdullah University of Science and Technology (KAUST), Physical Sciences and Engineering Division (PSE), Thuwal, Saudi Arabia

⁷Department of Electrical and Computer Engineering, University of Minnesota, Minneapolis, Minnesota 55455, USA



(Received 25 July 2022; accepted 13 January 2023; published 31 January 2023)

Exchange bias arises from the interfacial exchange coupling in ferromagnet-antiferromagnet bilayers and manifests as a horizontal shift of the magnetic hysteresis loop, constituting a critical component underpinning a broad range of magnetoresistive logic and memory devices. The facile implementation of exchange bias in van der Waals (vdW) magnets would be a key step towards practical devices for emerging vdW spintronics. Here, we report an easy approach to establishing strong exchange bias in the vdW magnet Fe_5GeTe_2 by a single-step process—atomic layer deposition (ALD) of oxides on Fe_5GeTe_2 . We successfully created exchange bias of 300–1500 Oe in $\text{Fe}_5\text{GeTe}_2/\text{Al}_2\text{O}_3$, $\text{Fe}_5\text{GeTe}_2/\text{ZnO}$, and $\text{Fe}_5\text{GeTe}_2/\text{V}_2\text{O}_5$ heterostructures, at 130 K. Control experiments showed that increasing the oxidant pulse duration in each ALD cycle or utilizing the stronger oxidant O_3 can enhance the exchange bias strength, revealing the key role of the ALD oxidants. Our systematic work elucidates the essential role of ALD-enabled oxidization of Fe_5GeTe_2 in the formation of exchange bias, and establishes ALD of oxides as a facile, controllable, and generally effective approach to creating giant exchange bias in vdW magnets, representing an integral advance towards practical vdW spintronic devices.

DOI: [10.1103/PhysRevMaterials.7.014008](https://doi.org/10.1103/PhysRevMaterials.7.014008)

I. INTRODUCTION

Exchange bias, a magnetic phenomenon emerging at the interface between a ferromagnet and an antiferromagnet, originates from the pinning of spins in the ferromagnetic (FM) layer by the adjacent antiferromagnetic (AFM) layer [1,2], effectively stabilizing the ferromagnet against the environmental stray magnetic fields. This phenomenon has been implemented in a wide range of technological applications including magnetic memories [3], magnetic read heads [4], and sensors [5], and plays the foundational role for advanced spintronics [6–12]. The recently emerged van der Waals (vdW) magnets [13–20] constitute unique platforms that promise the next generation of atomically thin magnetoelectric and magneto-optic devices; however, the large interlayer spacing poses a fundamental challenge in regard to how to establish strong exchange bias in vdW systems.

Thus far, the exchange bias has been studied in multiple vdW FM/AFM heterostructures including $\text{Fe}_3\text{GeTe}_2/\text{CrI}_3$ [21], $\text{Fe}_3\text{GeTe}_2/\text{FePS}_3$ [22], and $\text{Fe}_3\text{GeTe}_2/\text{MnPX}_3$ ($X = \text{S}$ and Se) [23,24], which all rely on the sophisticated stacking of

dissimilar vdW flakes, and have relatively small magnitudes of exchange bias (e.g., 200 Oe at 10 K in $\text{Fe}_3\text{GeTe}_2/\text{CrI}_3$). A facile approach that can generate strong exchange bias, while being compatible with the Si-based fabrication technology, is highly desirable. Recently, the exchange bias was observed in vdW FM Fe_3GeTe_2 after being annealed in the air [25], suggesting the possibility of using surface oxidation to convert FM Fe_3GeTe_2 layers into AFM oxidized Fe_3GeTe_2 . Compared with thermal annealing in the air with complex gases, atomic layer deposition (ALD) is a cleaner and more rigorous technique for surface reactions due to its use of pure gas precursors (e.g., H_2O or O_3) and the precise time control of each oxidant gas pulse. Moreover, ALD represents an industry-favored technique for growing ultrathin conformal dielectrics on electronic materials [26]. If the exchange bias can be created in vdW magnets by the ALD process, it would reveal not only useful knowledge for applying vdW magnets to spintronic and electronic devices but also practical guidance on device fabrication. In addition, given that the exchange bias in air-annealed Fe_3GeTe_2 still drops below 250 Oe at 100 K [25], new vdW magnets beyond Fe_3GeTe_2 should be explored to achieve strong exchange bias.

Recently, an itinerant vdW ferromagnet Fe_5GeTe_2 has garnered significant attention due to its higher magnetic ordering

*Corresponding author: gongc@umd.edu

temperature compared to Fe_3GeTe_2 [20,27]; meanwhile its exchange bias remains to be explored. Here, via growing nonmagnetic oxides by ALD, we demonstrate giant exchange bias in the vdW ferromagnet Fe_5GeTe_2 . Through reflectance magnetic circular dichroism (RMCD) studies, we found that the exchange bias in the $\text{Fe}_5\text{GeTe}_2/\text{Al}_2\text{O}_3$ structure reaches 460 Oe at 130 K after field cooling, and the effect persists at 160 K. The strong exchange bias was reproducible by ALD of ZnO and V_2O_5 on Fe_5GeTe_2 , suggesting that our ALD integration of exchange bias is generically effective. The exchange bias is potentially formed at the interface between oxidized Fe_5GeTe_2 (AFM) and unoxidized Fe_5GeTe_2 (FM) layers. Remarkably, by increasing the reaction time of oxidant H_2O with Fe_5GeTe_2 or utilizing O_3 as a stronger oxidant during ALD, we enhanced the exchange bias effectively (up to ~ 1500 Oe). These observations strongly suggest the critical role of initial oxidization in forming and enhancing exchange bias. Our results demonstrated a facile, controllable, and generally effective method to create giant exchange bias for vdW spintronics devices.

II. EXPERIMENTAL DETAILS

Bulk Fe_5GeTe_2 single crystals were synthesized by a chemical vapor transport method; the crystals of average composition near $\text{Fe}_{4.7(2)}\text{GeTe}_2$ were quenched by controlling the growth temperature and have a bulk Curie temperature (T_C) near 270–310 K [28]. Fe_5GeTe_2 flakes were mechanically exfoliated by scotch tape and transferred onto 260-nm-thick SiO_2/Si chips. Atomic force microscopy confirmed the thickness of Fe_5GeTe_2 flakes to be ~ 30 –80 nm. Temperature-dependent RMCD on an exfoliated pristine flake indicates a T_C of ~ 243 K (Fig. S1 in the Supplemental Material [29]). Consistent with the literature [20], the T_C of exfoliated flakes can be lowered by 30–40 K compared to the T_C of bulk Fe_5GeTe_2 (270–310 K). To avoid unwanted oxidation in the air, we stored the samples in a glovebox filled with N_2 gas, with oxygen and moisture levels < 0.1 ppm.

The $\text{Fe}_5\text{GeTe}_2/\text{oxide}$ heterostructures were prepared by ALD in a BENEQ TFS 500 reactor with a base pressure of 2 mbar. For ALD of Al_2O_3 , $\text{Al}(\text{CH}_3)_3$ and H_2O were used as the aluminum precursor and the oxidizing agent, respectively. The pulse of $\text{Al}(\text{CH}_3)_3$ or H_2O was controlled by regular ALD valves, which introduce N_2 to the precursor supply vessel, allowing the vapor pressure of $\text{Al}(\text{CH}_3)_3$ or H_2O to be established in the N_2 headspace, followed by the injection of the headspace gas to the downstream ALD valves. The 10-nm Al_2O_3 was grown at 150°C with 87 cycles, each consisting of 0.2-s $\text{Al}(\text{CH}_3)_3$ pulse, 0.5-s N_2 purge, 0.2-s H_2O pulse, and 0.5-s N_2 purge. For ALD of 10-nm-thick ZnO, all settings were kept the same as the Al_2O_3 growth including the H_2O pulse length of 200 ms, except that the ALD precursor became $\text{Zn}(\text{C}_2\text{H}_5)_2$. Last, for ALD of V_2O_5 , $\text{VO}(\text{OC}_3\text{H}_7)_3$ was used as the vanadium precursor, whereas ozone was the oxidant instead of water. A MKS O3MEGA ozone delivery subsystem was employed to provide a stable 17.3 wt % O_3 from a pure O_2 source. V_2O_5 of 10 nm was grown at 170°C with 222 cycles, each having 0.5-s $\text{VO}(\text{OC}_3\text{H}_7)_3$ pulse, 1-s N_2 purge, 2-s O_3 pulse, and 5-s N_2 purge as reported [30].

Furthermore, to study the impact of ALD oxidants on the exchange bias effect, we prepared $\text{Fe}_5\text{GeTe}_2/\text{Al}_2\text{O}_3$ samples with different pulse lengths of H_2O per ALD cycle (i.e., 200, 800, and 1600 ms) while keeping the rest of the parameters the same. To avoid the incomplete removal of H_2O , we set the N_2 purge to be 4 s instead of 0.5 s after the H_2O pulse for each ALD cycle. And we also compared the exchange bias in two $\text{Fe}_5\text{GeTe}_2/\text{Al}_2\text{O}_3$ heterostructures where Al_2O_3 was grown by different oxidants (i.e., H_2O vs O_3). For a fair comparison, the 10-nm Al_2O_3 was grown at 150°C with 87 cycles, each consisting of 0.2-s $\text{Al}(\text{CH}_3)_3$ pulse, 0.5-s N_2 purge, 0.2-s H_2O or O_3 pulse, and 0.5-s N_2 purge.

The sample's out-of-plane magnetization was probed by RMCD under the out-of-plane magnetic field up to 300 mT in a Montana cryostat ($< 10^{-4}$ Torr). A HeNe laser (633 nm, optical power of $7\ \mu\text{W}$) was focused onto the samples via a $50\times$ objective of numerical aperture 0.5 to achieve a submicrometer spot size. A photoelastic modulator at 50 kHz was used to modulate the helicity of the optical excitation between left and right, and a photodiode detected the reflected light from the sample. The RMCD was determined by the ratio between an AC signal at 50 kHz and a low-frequency AC signal at 237 Hz of the reflected light intensity, which was measured by two different lock-in amplifiers.

III. RESULTS AND DISCUSSION

Figure 1(a) shows a schematic of the Fe_5GeTe_2 crystal structure with three-layer periodicity along the c axis (out-of-plane direction), where nonequivalent Fe sites are labeled as Fe(1), Fe(2), and Fe(3). Two locations of Fe(1) represent the split sites, and their occupation (either up or down) leads to the adjustment of the Ge atom (down or up, respectively). Thus, the crystal structure of Fe_5GeTe_2 was found to be more complex than Fe_3GeTe_2 due to those split sites and vacancy disorder [20]. In this work, Fe_5GeTe_2 flakes (~ 30 –80 nm thick) with lateral areas above $8 \times 8\ \mu\text{m}^2$ were mechanically exfoliated from bulk crystals onto the Si substrates with 260-nm-thick SiO_2 , and subsequently examined by optical microscopy [Fig. 1(b)]. Raman spectroscopy of Fe_5GeTe_2 [Fig. 1(c)] shows the A_{1g} peak ($123\ \text{cm}^{-1}$) and the combined $A_{1g} + E_{2g}$ peak ($153\ \text{cm}^{-1}$), similar to the Fe_3GeTe_2 feature [31]. For a pristine Fe_5GeTe_2 flake, its out-of-plane magnetization was probed by RMCD at 130 K after zero-field cooling (ZFC). As expected, the magnetic hysteresis loop remains symmetric to the zero magnetic field [Fig. 1(d)], indicating the absence of exchange bias in pristine Fe_5GeTe_2 .

Next, 10-nm-thick Al_2O_3 was grown by ALD on top of Fe_5GeTe_2 , involving surface chemical reactions between the metal precursor $\text{Al}(\text{CH}_3)_3$ and the oxidant H_2O [32,33]. The magnetic hysteresis loops of a $\text{Fe}_5\text{GeTe}_2/\text{Al}_2\text{O}_3$ heterostructure were then measured by RMCD at 130 K after the positive- and negative-field cooling (PFC and NFC), respectively. In stark contrast to the pristine Fe_5GeTe_2 that has a symmetric magnetic hysteresis loop [Fig. 1(d)], significant loop shifts of the $\text{Fe}_5\text{GeTe}_2/\text{Al}_2\text{O}_3$ heterostructure after PFC and NFC clearly confirm the emergence of exchange bias [Fig. 1(e)], with the exchange bias field (H_{ex}) being negative (positive) after PFC (NFC) as expected [2]. We observed the exchange bias at 130 K in multiple $\text{Fe}_5\text{GeTe}_2/\text{Al}_2\text{O}_3$

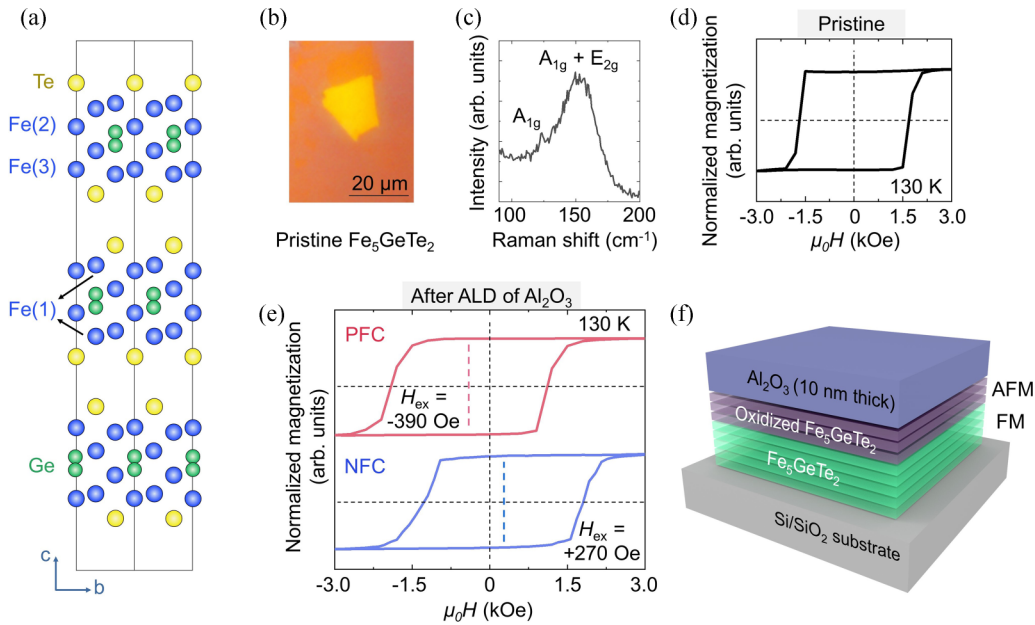


FIG. 1. Characterizations of Fe_5GeTe_2 and $\text{Fe}_5\text{GeTe}_2/\text{Al}_2\text{O}_3$. (a) Side view of Fe_5GeTe_2 crystal structure where Fe(1) and Ge are split sites. The optical image (b) and Raman spectrum (c) of a pristine Fe_5GeTe_2 flake. (d) RMCD measurement of the out-of-plane magnetization of the pristine Fe_5GeTe_2 at 130 K after ZFC. The vertical and horizontal black dashed lines serve as the eye guide for zero magnetic field ($x = 0$) and zero magnetization ($y = 0$), respectively. No exchange bias was found in pristine Fe_5GeTe_2 . (e) RMCD measurements of a representative $\text{Fe}_5\text{GeTe}_2/\text{Al}_2\text{O}_3$ heterostructure at 130 K after PFC and NFC, respectively. The red (blue) dashed line highlights the shifted center line of the magnetic hysteresis loop after PFC (NFC). The magnitude of the cooling field is 3000 Oe in this study. After ALD of 10-nm-thick Al_2O_3 on Fe_5GeTe_2 , negative (positive) exchange bias emerges after PFC (NFC) in the heterostructure. (f) Schematics of the $\text{Fe}_5\text{GeTe}_2/\text{Al}_2\text{O}_3$ heterostructure consisting of oxidized Fe_5GeTe_2 . The Fe_5GeTe_2 layers at the $\text{Fe}_5\text{GeTe}_2/\text{Al}_2\text{O}_3$ interface are likely oxidized upon ALD and serve as the antiferromagnetic pinning layers to induce the exchange bias effect.

heterostructures after PFC and NFC (Fig. S2 in the Supplemental Material [29]), suggesting that the phenomena are well reproducible. As further evidence, exchange bias also appears in $\text{Fe}_5\text{GeTe}_2/\text{Al}_2\text{O}_3$ heterostructures after the first ZFC, with random signs and amplitudes (Fig. S3 in the Supplemental Material [29]). Because Al_2O_3 itself is nonmagnetic, the observed exchange bias indicates the AFM nature of the oxidized Fe_5GeTe_2 layers formed upon ALD of Al_2O_3 , as illustrated by Fig. 1(f). This agrees with the recent report of exchange bias in the vdW magnet Fe_3GeTe_2 after being annealed in the air at 100°C for 30 min [25].

We continued to systematically examine the temperature dependence of the magnetic hysteresis loops and the exchange bias in a representative $\text{Fe}_5\text{GeTe}_2/\text{Al}_2\text{O}_3$ heterostructure. As shown in Fig. 2(a), raising the temperature decreases the coercivity (H_c) by introducing stronger thermal fluctuations, and the hysteresis loop finally disappears at 190 K. The decreasing trend is also observed for H_{ex} as the temperature increases [Fig. 2(d)]. Notably, H_{ex} reaches 460 Oe at 130 K after NFC and persists to 160 K with a magnitude of 50 Oe, indicating a blocking temperature (T_B) around 160–170 K at which the exchange bias disappears. In short, these results suggest that ALD of Al_2O_3 on top of Fe_5GeTe_2 leads to a strong exchange bias with a relatively high T_B .

To prove that our method to generate exchange bias is not oxide specific, we extended to ALD of ZnO [34] and V_2O_5 [30], as illustrated by the top schematics in Fig. 2. Indeed, magnetic hysteresis loops with large positive shifts were observed after NFC for both $\text{Fe}_5\text{GeTe}_2/\text{ZnO}$

and $\text{Fe}_5\text{GeTe}_2/\text{V}_2\text{O}_5$ heterostructures. For $\text{Fe}_5\text{GeTe}_2/\text{ZnO}$, the hysteresis loop shrinks with the increasing temperature and disappears at ~ 160 K [Fig. 2(b)]. H_{ex} reaches 1007 Oe at 130 K, decreases gradually as the temperature increases, and remains at 710 Oe when H_c drops to zero at 160 K [Fig. 2(e)]. For $\text{Fe}_5\text{GeTe}_2/\text{V}_2\text{O}_5$, H_{ex} persists at the level of ~ 1500 Oe to at least 170 K [Figs. 2(c) and 2(f)], showing an even stronger exchange bias effect compared to $\text{Fe}_5\text{GeTe}_2/\text{Al}_2\text{O}_3$ and $\text{Fe}_5\text{GeTe}_2/\text{ZnO}$ in this work. Remarkably, such a large H_{ex} in $\text{Fe}_5\text{GeTe}_2/\text{V}_2\text{O}_5$ is 600–1000 Oe greater than the reported H_{ex} in other vdW magnets [21–25,35] and is achievable at high temperatures (e.g., 150–170 K). The general existence of exchange bias in $\text{Fe}_5\text{GeTe}_2/\text{oxides}$ fabricated by ALD further suggests the scenario that the observed exchange bias is due to the oxidation of top Fe_5GeTe_2 layers during the ALD process.

In addition, there is no noticeable dependence of the exchange bias strength on the Fe_5GeTe_2 layer thickness in $\text{Fe}_5\text{GeTe}_2/\text{oxides}$ (Fig. S4 in the Supplemental Material [29]). This finding is in contrast to the observations in conventional FM/AFM bilayer systems where H_{ex} magnitude depends inversely on the FM thickness [2], but agrees with the recent observations on the exchange bias in vdW magnet Fe_3GeTe_2 [21,25], showing a unique magnetic behavior due to the weak interlayer exchange coupling inherent to layered vdW magnets. Therefore, the thickness variance among Fe_5GeTe_2 samples should not interfere with the major finding that the exchange bias in $\text{Fe}_5\text{GeTe}_2/\text{oxides}$ is mainly due to the ALD-induced oxidation in Fe_5GeTe_2 . Overall, these observations trigger an interesting question regarding whether we can

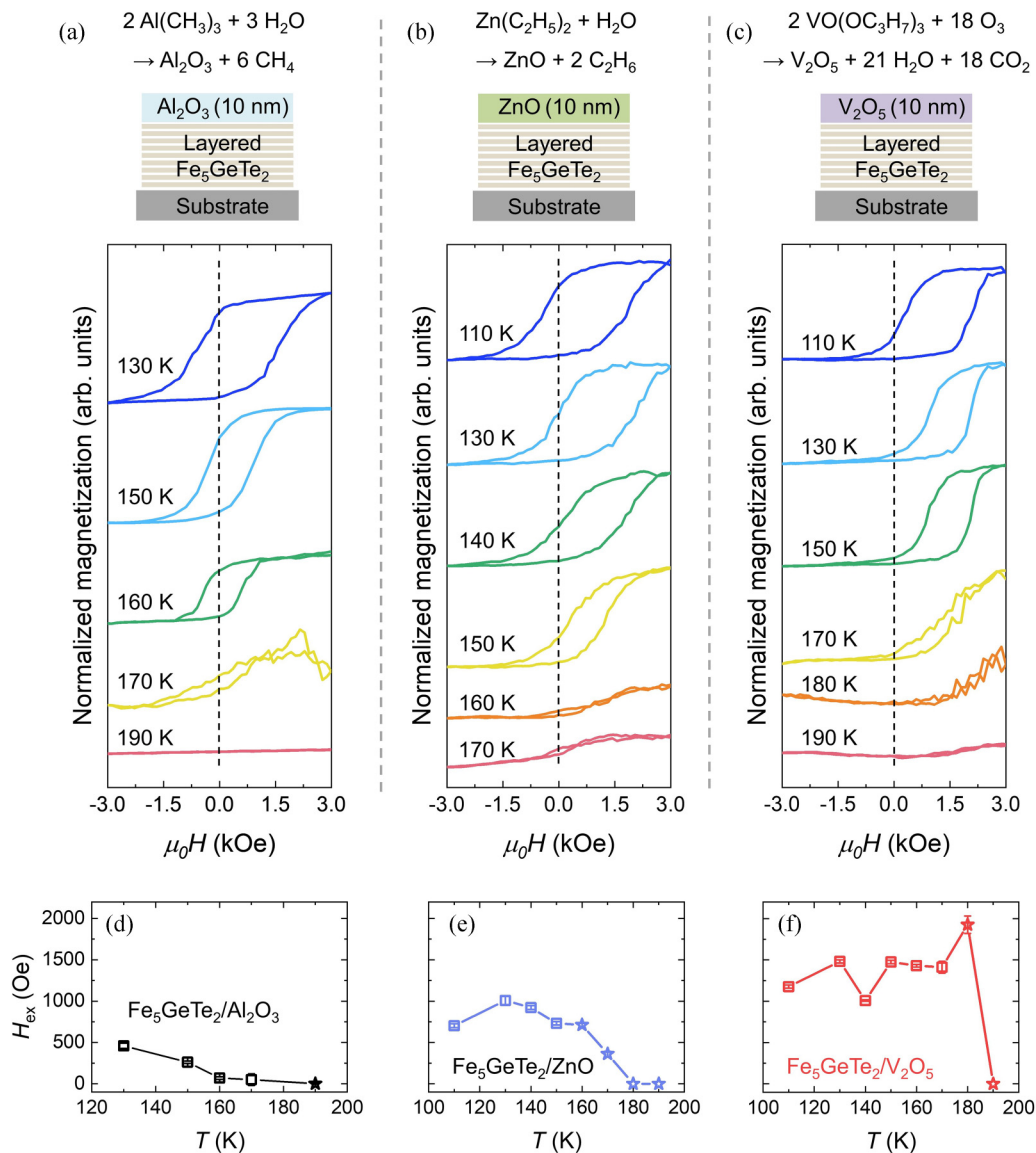


FIG. 2. Temperature dependence of the exchange bias in three types of $\text{Fe}_5\text{GeTe}_2/\text{oxide}$ heterostructures. (a)–(c) Temperature dependence of magnetic hysteresis loops measured by RMCD in three types of $\text{Fe}_5\text{GeTe}_2/\text{oxide}$ heterostructures: $\text{Fe}_5\text{GeTe}_2/\text{Al}_2\text{O}_3$ (a), $\text{Fe}_5\text{GeTe}_2/\text{ZnO}$ (b), and $\text{Fe}_5\text{GeTe}_2/\text{V}_2\text{O}_5$ (c). Positive shifts of hysteresis loops emerge after NFC for all $\text{Fe}_5\text{GeTe}_2/\text{oxides}$ systems. The black dashed lines serve as the eye guide for zero magnetic field ($x = 0$). The corresponding ALD reactions for each type of $\text{Fe}_5\text{GeTe}_2/\text{oxide}$ are illustrated in the top schematics. (d)–(f) The exchange bias H_{ex} as a function of temperature for the three types of $\text{Fe}_5\text{GeTe}_2/\text{oxides}$. To indicate the possible uncertainty in extracted values, H_{ex} data points are marked by stars when the coercivity drops to zero. Error bars represent the standard deviation above the mean of the extracted data.

control the exchange bias strength in Fe_5GeTe_2 by tuning the ALD conditions.

It is worth highlighting that the ALD of V_2O_5 adopted O_3 [Figs. 2(c) and 2(f)], a stronger oxidant than H_2O , and the resultant exchange bias in $\text{Fe}_5\text{GeTe}_2/\text{V}_2\text{O}_5$ are clearly stronger than that in $\text{Fe}_5\text{GeTe}_2/\text{Al}_2\text{O}_3$ [Figs. 2(a) and 2(d)] and $\text{Fe}_5\text{GeTe}_2/\text{ZnO}$ [Figs. 2(b) and 2(e)]. This again indicates the critical role of ALD-enabled oxidization of Fe_5GeTe_2 in the final formation of exchange bias. We conducted two sets of control experiments to unravel the underlying mechanism further. First, using $\text{Fe}_5\text{GeTe}_2/\text{Al}_2\text{O}_3$ as the model system, we varied the ALD pulse duration of oxidant H_2O and studied its impact on the exchange bias strength (see Experimental Details). We increased the H_2O pulse duration per cycle from

200 to 1600 ms while keeping the rest of the parameters the same [e.g., temperature, pulse duration of the precursor $\text{Al}(\text{CH}_3)_3$, and cycle numbers]. In Fig. 3(a), we summarized all the H_{ex} measured at 130 K after NFC on randomly selected multiple samples for each H_2O pulse duration. By increasing the H_2O pulse duration from 200 to 1600 ms, H_{ex} increases by about 170% from 290 ± 130 to 790 ± 230 Oe [Fig. 3(a)], demonstrating an effective tuning of the resultant exchange bias strength by adjusting the ALD oxidant's pulse duration.

As a second set of control experiments, we studied the exchange bias strengths in $\text{Fe}_5\text{GeTe}_2/\text{Al}_2\text{O}_3$ samples prepared by two different ALD oxidants (i.e., H_2O versus O_3) while maintaining all other ALD parameters the same. Un-

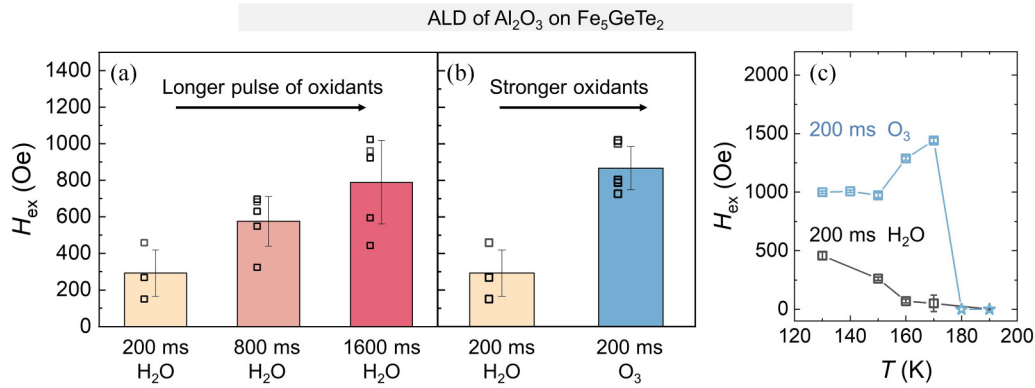


FIG. 3. Tuning the exchange bias strength in Fe₅GeTe₂/Al₂O₃ heterostructures by adjusting the oxidants during ALD. (a),(b) Summary of H_{ex} in Fe₅GeTe₂/Al₂O₃ heterostructures where oxides were prepared using the H₂O pulse durations of 200, 800, and 1600 ms per ALD cycle (a) or using different ALD oxidants (i.e., H₂O vs O₃) (b). For each set of Fe₅GeTe₂/Al₂O₃ heterostructures, three to five randomly selected sample flakes were measured at 130 K after NFC to show the variance. The average H_{ex} for each set is shown by the histogram, with the original data points shown on the left and the error bar representing the standard deviation above the mean on top of each histogram. The resultant exchange bias is effectively enhanced by increasing the pulse duration of the ALD oxidant (i.e., longer H₂O pulse) or utilizing O₃ as a stronger oxidant during ALD of Al₂O₃. (c) The exchange bias H_{ex} after NFC as a function of temperature for Fe₅GeTe₂/Al₂O₃ prepared by H₂O and O₃. To indicate the possible uncertainty in extracted values, H_{ex} data points are marked by stars when the coercivity drops to zero. Error bars represent one standard deviation above the mean of the extracted data.

der the same oxidant pulse duration of 200 ms, the statistic study summarized in Fig. 3(b) shows that H_{ex} increases from an average of 290 ± 130 to 870 ± 120 Oe by switching from H₂O to O₃, with a percentage increase of 200%. Moreover, we measured the temperature dependence of H_{ex} in Fe₅GeTe₂/Al₂O₃ prepared by O₃ (hysteresis loops in Fig. S5 in the Supplemental Material [29]) and compared the H_{ex} results with Fe₅GeTe₂/Al₂O₃ prepared by H₂O in Fig 3(c). The maximum H_{ex} reaches 1450 Oe at 170 K after NFC for Fe₅GeTe₂/Al₂O₃ prepared by O₃, which is comparable with that achieved at 170 K in O₃-prepared Fe₅GeTe₂/V₂O₅ [see Fig. 2(f)] but about three times larger than the maximum exchange bias obtained at 130 K in Fe₅GeTe₂/Al₂O₃ prepared by H₂O. This result suggests that ALD oxidants (i.e., O₃ and H₂O) play a major role in determining the exchange bias strength. It has been well established that O₃, as a stronger oxidant, can react more with the basal plane of many vdW materials than H₂O during the nucleation stage of ALD [26,36–38]. Thus, similar effects by O₃ are expected for ALD of oxides on the vdW magnets in this work, which could lead to a stronger oxidation to enhance the exchange bias effect.

The giant exchange bias in Fe₅GeTe₂/oxides discovered in this work has been exceptional for vdW magnets. In Fig. 4, we summarized the maximum values of H_{ex} measured in vdW magnets/heterostructures and their measurement temperatures. For many all-vdW heterostructures, H_{ex} exceeding 200 Oe can only be achieved at low temperatures (e.g., 10 K) [21,23,24,35]. In contrast, H_{ex} with the maximum magnitude in the range 400–1000 Oe at 130 K can be easily induced in Fe₅GeTe₂ by ALD of Al₂O₃ or ZnO using the oxidant H₂O with varying H₂O pulse durations. By means of a stronger oxidant O₃, the maximum values of H_{ex} reach ~1500 Oe at 170 K in Fe₅GeTe₂/V₂O₅ and Fe₅GeTe₂/Al₂O₃ heterostructures, which are about 1000 Oe larger than the reported H_{ex} in most Fe₃GeTe₂-based heterostructures as summarized in Fig. 4.

IV. CONCLUSIONS

In summary, we utilized ALD of oxides to achieve a facile integration of giant exchange bias in vdW magnet Fe₅GeTe₂. Through ALD of Al₂O₃, we induced a sizable exchange bias of 460 Oe at 130 K. The exchange bias effect is reproducible by ALD of two other oxides (ZnO and V₂O₅), confirming the general effectiveness of our approach. Through control experiments, we demonstrated that the exchange bias strength can be enhanced by increasing the oxidant pulse duration in each ALD cycle or utilizing the stronger oxidant O₃. In particular, the maximum exchange

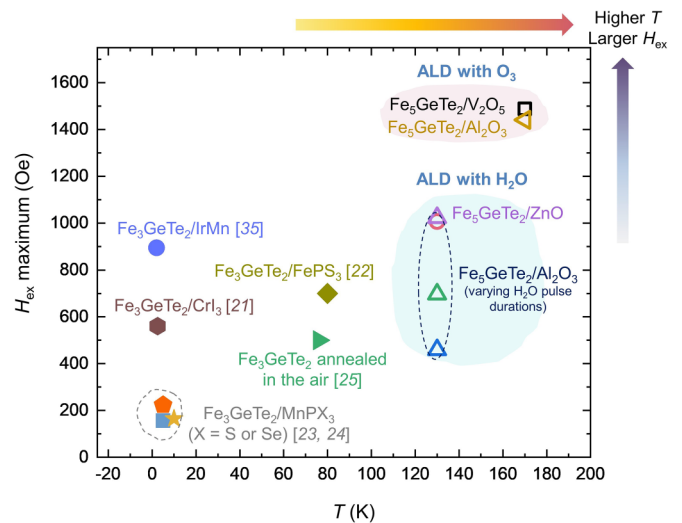


FIG. 4. The maximum exchange bias versus the measurement temperature for different vdW magnets and heterostructures (data adapted from Refs. [21–25,35]). H_{ex} data of this work when H_c becomes zero are not included. The exchange bias in our Fe₅GeTe₂/oxide is strong and retained at relatively high temperatures.

bias reaches ~ 1500 Oe at 170 K for $\text{Fe}_5\text{GeTe}_2/\text{V}_2\text{O}_5$ and $\text{Fe}_5\text{GeTe}_2/\text{Al}_2\text{O}_3$ that were both prepared by O_3 , about three times larger than the maximum exchange bias achieved at 130 K for $\text{Fe}_5\text{GeTe}_2/\text{Al}_2\text{O}_3$ by H_2O , highlighting the critical role of the ALD oxidants in the formation of the exchange bias. Our results demonstrate a method that is simple, generally effective, and integrable to the existing Si-based fabrication technology, for creating giant exchange bias persisting up to relatively high temperatures in Fe_5GeTe_2 . This ALD-based method allows a one-step integration of giant exchange bias during dielectric growth for simple device assembly, beneficial for ultracompact vdW spintronics devices. We envision that the future optimization of this approach could benefit from the advancement in unraveling the detailed relationship between the chemical, atomic, and magnetic properties of the oxide phase at the interface. Our discovery of the one-step ALD integration of giant exchange bias in Fe_5GeTe_2

represents an important step towards practical vdW spintronic devices.

ACKNOWLEDGMENTS

C.G. acknowledges the grant support from Air Force Office of Scientific Research under Award No. FA9550-22-1-0349, Naval Air Warfare Center Aircraft Division under Award No. N00421-22-1-0001, Army Research Laboratory under Cooperative Agreement No. W911NF-19-2-0181, and National Science Foundation under Awards No. CMMI-2233592 and No. 49100423C0011. Bulk Fe_5GeTe_2 crystal synthesis and characterization (A.F.M. and M.A.M.) were supported by the U. S. Department of Energy, Office of Science, Basic Energy Sciences, Materials Sciences and Engineering Division. J.-P.W. acknowledges the support of Robert F. Hartmann Endowed Chair Professorship.

-
- [1] W. H. Meiklejohn and C. P. Bean, New magnetic anisotropy, *Phys. Rev.* **102**, 1413 (1956).
- [2] J. Nogués and I. K. Schuller, Exchange bias, *J. Magn. Magn. Mater.* **192**, 203 (1999).
- [3] I. L. Prejbeanu, W. Kula, K. Ounadjela, R. C. Sousa, O. Redon, B. Dieny, and J.-P. Nozieres, Thermally assisted switching in exchange-biased storage layer magnetic tunnel junctions, *IEEE Trans. Magn.* **40**, 2625 (2004).
- [4] C. H. Tsang, R. E. Fontana, T. Lin, D. E. Heim, B. A. Gurney, and M. L. Williams, Design, fabrication, and performance of spin-valve read heads for magnetic recording applications, *IBM J. Res. Dev.* **42**, 103 (1998).
- [5] C. Binek and B. Doudin, Magnetoelectronics with magnetoelectrics, *J. Phys.: Condens. Matter* **17**, L39 (2005).
- [6] C. Chappert, A. Fert, and F. N. Van Dau, The emergence of spin electronics in data storage, *Nat. Mater.* **6**, 813 (2007).
- [7] T. Jungwirth, X. Marti, P. Wadley, and J. Wunderlich, Antiferromagnetic spintronics, *Nat. Nanotechnol.* **11**, 231 (2016).
- [8] P. H. Lin, B. Y. Yang, M. H. Tsai, P. C. Chen, K. F. Huang, H. H. Lin, and C. H. Lai, Manipulating exchange bias by spin-orbit torque, *Nat. Mater.* **18**, 335 (2019).
- [9] S. Peng, D. Zhu, W. Li, H. Wu, A. J. Grutter, D. A. Gilbert, J. Lu, D. Xiong, W. Cai, P. Shafer, K. L. Wang, and W. Zhao, Exchange bias switching in an antiferromagnet/ferromagnet bilayer driven by spin-orbit torque, *Nat. Electron.* **3**, 757 (2020).
- [10] M. Gibert, P. Zubko, R. Scherwitzl, J. Íñiguez, and J. M. Triscone, Exchange bias in LaNiO_3 - LaMnO_3 superlattices, *Nat. Mater.* **11**, 195 (2012).
- [11] Y. Fan, K. J. Smith, G. Lüpke, A. T. Hanbicki, R. Goswami, C. H. Li, H. B. Zhao, and B. T. Jonker, Exchange bias of the interface spin system at the Fe/MgO interface, *Nat. Nanotechnol.* **8**, 438 (2013).
- [12] E. Maniv, R. A. Murphy, S. C. Haley, S. Doyle, C. John, A. Maniv, S. K. Ramakrishna, Y.-L. Tang, P. Ercius, R. Ramesh, A. P. Reyes, J. R. Long, and J. G. Analytis, Exchange bias due to coupling between coexisting antiferromagnetic and spin-glass orders, *Nat. Phys.* **17**, 525 (2021).
- [13] C. Gong, L. Li, Z. Li, H. Ji, A. Stern, Y. Xia, T. Cao, W. Bao, C. Wang, Y. Wang, Z. Q. Qiu, R. J. Cava, S. G. Louie, J. Xia, and X. Zhang, Discovery of intrinsic ferromagnetism in two-dimensional van der Waals crystals, *Nature (London)* **546**, 265 (2017).
- [14] B. Huang, G. Clark, E. Navarro-Moratalla, D. R. Klein, R. Cheng, K. L. Seyler, D. Zhong, E. Schmidgall, M. A. McGuire, D. H. Cobden, W. Yao, D. Xiao, P. Jarillo-Herrero, and X. Xu, Layer-dependent ferromagnetism in a van der Waals crystal down to the monolayer limit, *Nature (London)* **546**, 270 (2017).
- [15] C. Gong and X. Zhang, Two-dimensional magnetic crystals and emergent heterostructure devices, *Science* **363**, eaav4450 (2019).
- [16] K. S. Burch, D. Mandrus, and J. G. Park, Magnetism in two-dimensional van der Waals materials, *Nature (London)* **563**, 47 (2018).
- [17] M. Gibertini, M. Koperski, A. F. Morpurgo, and K. S. Novoselov, Magnetic 2D materials and heterostructures, *Nat. Nanotechnol.* **14**, 408 (2019).
- [18] Z. Fei, B. Huang, P. Malinowski, W. Wang, T. Song, J. Sanchez, W. Yao, D. Xiao, X. Zhu, A. F. May, W. Wu, D. H. Cobden, J.-H. Chu, and X. Xu, Two-dimensional itinerant ferromagnetism in atomically thin Fe_3GeTe_2 , *Nat. Mater.* **17**, 778 (2018).
- [19] Y. Deng, Y. Yu, Y. Song, J. Zhang, N. Z. Wang, Z. Sun, Y. Yi, Y. Z. Wu, S. Wu, J. Zhu, J. Wang, X. H. Chen, and Y. Zhang, Gate-tunable room-temperature ferromagnetism in two-dimensional Fe_3GeTe_2 , *Nature (London)* **563**, 94 (2018).
- [20] A. F. May, D. Ovchinnikov, Q. Zheng, R. Hermann, S. Calder, B. Huang, Z. Fei, Y. Liu, X. Xu, and M. A. McGuire, Ferromagnetism near room temperature in the cleavable van der Waals crystal Fe_3GeTe_2 , *ACS Nano* **13**, 4436 (2019).
- [21] R. Zhu, W. Zhang, W. Shen, P. K. J. Wong, Q. Wang, Q. Liang, Z. Tian, Y. Zhai, C. W. Qiu, and A. T. S. Wee, Exchange bias in van der Waals $\text{CrCl}_3/\text{Fe}_3\text{GeTe}_2$ heterostructures, *Nano Lett.* **20**, 5030 (2020).
- [22] L. Zhang, X. Huang, H. Dai, M. Wang, H. Cheng, L. Tong, Z. Li, X. Han, X. Wang, L. Ye, and J. Han, Proximity-coupling-induced significant enhancement of coercive field and curie temperature in 2D van der Waals heterostructures, *Adv. Mater.* **32**, 2002032 (2020).

- [23] G. Hu, Y. Zhu, J. Xiang, T. Y. Yang, M. Huang, Z. Wang, Z. Wang, P. Liu, Y. Zhang, C. Feng, D. Hou, W. Zhu, M. Gu, C. H. Hsu, F. C. Chuang, Y. Lu, B. Xiang, and Y. L. Chueh, Antisymmetric magnetoresistance in a van der Waals antiferromagnetic/ferromagnetic layered $\text{MnPS}_3/\text{Fe}_3\text{GeTe}_2$ stacking heterostructure, *ACS Nano* **14**, 12037 (2020).
- [24] H. Dai, H. Cheng, M. Cai, Q. Hao, Y. Xing, H. Chen, X. Chen, X. Wang, and J. B. Han, Enhancement of the coercive field and exchange bias effect in $\text{Fe}_3\text{GeTe}_2/\text{MnPX}_3$ ($X = \text{S}$ and Se) van der Waals heterostructures, *ACS Appl. Mater. Interfaces* **13**, 24314 (2021).
- [25] H. K. Gweon, S. Y. Lee, H. Y. Kwon, J. Jeong, H. J. Chang, K. W. Kim, Z. Q. Qiu, H. Ryu, C. Jang, and J. W. Choi, Exchange bias in weakly interlayer-coupled van der Waals magnet Fe_3GeTe_2 , *Nano Lett.* **21**, 1672 (2021).
- [26] H. G. Kim and H.-B.-R. Lee, Atomic layer deposition on 2D materials, *Chem. Mater.* **29**, 3809 (2017).
- [27] J. Seo, D. Y. Kim, E. S. An, K. Kim, G.-Y. Kim, S.-Y. Hwang, D. W. Kim, B. G. Jang, H. Kim, G. Eom, S. Y. Seo, R. Stania, M. Muntwiler, J. Lee, K. Watanabe, T. Taniguchi, Y. J. Jo, J. Lee, B. I. Min, M. H. Jo *et al.*, Nearly room temperature ferromagnetism in a magnetic metal-rich van der Waals metal, *Sci. Adv.* **6**, eaay8912 (2020).
- [28] A. F. May, C. A. Bridges, and M. A. McGuire, Physical properties and thermal stability of $\text{Fe}_{5-x}\text{GeTe}_2$ single crystals, *Phys. Rev. Mater.* **3**, 104401 (2019).
- [29] See Supplemental Material at <http://link.aps.org/supplemental/10.1103/PhysRevMaterials.7.014008> for T_C measurement, AFM images for thickness measurements, and exchange bias in multiple $\text{Fe}_5\text{GeTe}_2/\text{oxides}$ heterostructures.
- [30] X. Chen, E. Pomerantseva, P. Banerjee, K. Gregorczyk, R. Ghodssi, and G. Rubloff, Ozone-based atomic layer deposition of crystalline V_2O_5 films for high performance electrochemical energy storage, *Chem. Mater.* **24**, 1255 (2012).
- [31] L. Du, J. Tang, Y. Zhao, X. Li, R. Yang, X. Hu, X. Y. Bai, X. Wang, K. Watanabe, T. Taniguchi, D. Shi, G. Yu, X. Bai, T. Hasan, G. Zhang, and Z. Sun, Lattice dynamics, phonon chirality, and spin-phonon coupling in 2D itinerant ferromagnet Fe_3GeTe_2 , *Adv. Funct. Mater.* **29**, 1 (2019).
- [32] M. D. Groner, J. W. Elam, F. H. Fabreguette, and S. M. George, Electrical characterization of thin Al_2O_3 films grown by atomic layer deposition on silicon and various metal substrates, *Thin Solid Films* **413**, 186 (2002).
- [33] B. Lee, S.-Y. Park, H.-C. Kim, K. Cho, E. M. Vogel, M. J. Kim, R. M. Wallace, and J. Kim, Conformal Al_2O_3 dielectric layer deposited by atomic layer deposition for graphene-based nanoelectronics, *Appl. Phys. Lett.* **92**, 203102 (2008).
- [34] E. Guziewicz, M. Godlewski, L. Wachnicki, T. A. Krajewski, G. Luka, S. Gieraltowska, R. Jakiela, A. Stonert, W. Lisowski, M. Krawczyk, J. W. Sobczak, and A. Jablonski, ALD grown zinc oxide with controllable electrical properties, *Semicond. Sci. Technol.* **27**, 074011 (2012).
- [35] Y. Zhang, H. Xu, C. Yi, X. Wang, Y. Huang, J. Tang, J. Jiang, C. He, M. Zhao, T. Ma, J. Dong, C. Guo, J. Feng, C. Wan, H. Wei, H. Du, Y. Shi, G. Yu, G. Zhang, and X. Han, Exchange bias and spin-orbit torque in the Fe_3GeTe_2 -based heterostructures prepared by vacuum exfoliation approach, *Appl. Phys. Lett.* **118**, 262406 (2021).
- [36] Y. Xuan, Y. Q. Wu, T. Shen, M. Qi, M. A. Capano, J. A. Cooper, and P. D. Ye, Atomic-layer-deposited nanostructures for graphene-based nanoelectronics, *Appl. Phys. Lett.* **92**, 013101 (2008).
- [37] H. Liu, K. Xu, X. Zhang, and P. D. Ye, The integration of high-k dielectric on two-dimensional crystals by atomic layer deposition, *Appl. Phys. Lett.* **100**, 152115 (2012).
- [38] S. Jandhyala, G. Mordi, B. Lee, G. Lee, C. Floresca, P.-R. Cha, J. Ahn, R. M. Wallace, Y. J. Chabal, M. J. Kim, L. Colombo, K. Cho, and J. Kim, Atomic layer deposition of dielectrics on graphene using reversibly physisorbed ozone, *ACS Nano* **6**, 2722 (2012).